

## Saturation and forward jets at HERA

C. Marquet and R. Peschanski<sup>y</sup>Service de physique théorique, CEA/Saclay, 91191 Gif-sur-Yvette cedex, France<sup>z</sup>C. Royon<sup>x</sup>

Service de physique des particules, CEA/Saclay, 91191 Gif-sur-Yvette cedex, France

We analyse forward-jet production cross-sections at HERA in the framework of the Golec-Biernat and Wustho saturation models. We obtain a good description of the forward jet cross sections measured by the H1 and ZEUS collaborations in the two-hard-scale region ( $k_T \sim Q \sim Q_{\text{CD}}$ ) with two different parametrizations with either significant or weak saturation effects. The weak saturation parametrization gives a scale compatible with the one found for the proton structure function  $F_2$ . We argue that Mueller-Navelet jets at the Tevatron and the LHC could help distinguishing between both options.

## I. INTRODUCTION

The saturation regime describes the high-density phase of partons in perturbative QCD. It may occur for instance when the Balitsky-Fadin-Kuraev-Lipatov (BFKL) QCD evolution equation [1] goes beyond some energy related to the unitarity limit [2, 3, 4, 5, 6, 7]. On a phenomenological ground, a well-known saturation model [8] by Golec-Biernat and Wustho (GBW) gives a parametrization of the proton structure functions already in the HERA energy range. It provides a simple and elegant formulation of the transition to saturation. However, there does not yet exist a clear confirmation of saturation since the same data can well be explained within the conventional perturbative QCD framework [9].

In fact, the study of the proton structure functions is a one-hard-scale analysis process since their QCD properties are dominated by the evolution from a soft scale (the proton scale) to the hard scale of deep inelastic scattering. In order to favor the evolution at fixed transverse scale, which is expected to lead more directly to saturation, it seems interesting to focus on two-hard-scale processes such as forward-jet production at HERA, in the region where the transverse momentum of the jet  $k_T$  is of the order of the virtuality of the photon  $Q^2$  and where the rapidity interval for soft radiation is large. This kinematical configuration which was already proposed [10] for testing the BFKL evolution is thus also a good testing ground for saturation. The goal of our paper is then to formulate and study the extension of the GBW model to forward jets.

Among the physics questions that we want to raise, we analyse whether saturation effects can be sizeable in forward jets at HERA and whether they are compatible or not with the GBW parametrization of  $F_2$ : More generally, we would like to compare potential saturation effects in one-scale and two-scale processes. Indeed, in the two-scale process initiated by  $\gamma\gamma$  scattering, it has been suggested [11] that the saturation scale could be different and in fact quite larger than the one of deep inelastic scattering. However, another study of  $\gamma\gamma$  scattering sticks to the same saturation scale as for  $\gamma p$  scattering [12]. We will discuss this point with forward-jet data which have better statistics and wider kinematical range. This is of particular interest in the prospect of Mueller-Navelet jets [13] at the Tevatron and the LHC where saturation could play a bigger role.

The plan of the paper is the following. In Section 2, we formulate the extension of the GBW model for forward jets. In Section 3, we present the fitting method and give the results of the fits together with several tests of both saturation solutions that we obtain. Section 4 is devoted to a discussion of our results and to predictions for Mueller-Navelet jets at hadron colliders that could discriminate between both solutions.

<sup>z</sup> URA 2306, unité de recherche associée au CNRS.

E-mail address: marquet@spht.saclay.cea.fr

<sup>y</sup>E-mail address: pesch@spht.saclay.cea.fr<sup>x</sup>E-mail address: royon@hep.saclay.cea.fr

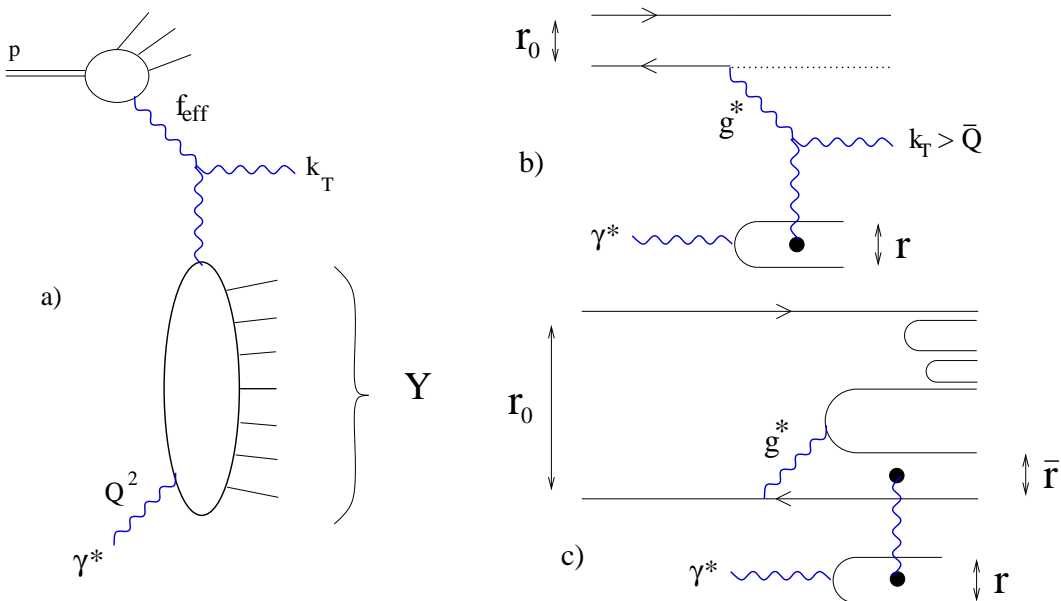


FIG. 1: Forward-jet production in partonic and dipole representations. Fig 1a: Forward jets at HERA. Fig 1b: Forward jet in onium scattering in the partonic representation (1st order i.e. with one gluon-exchange ( ))). Fig 1c: Forward jet in onium scattering in the dipole representation.  $Y$  : rapidity gap between the two hard probes.  $k_T > Q$  : jet transverse momentum lower bound.  $Q$  : virtuality of the photon. The gluon-dipole couplings are sketched by black points.

## II. FORMULATION

The original GBW model provides a simple formulation of the dipole-proton cross-section in terms of a saturation scale  $R_0(Y) = e^{-\frac{1}{2}(Y - Y_0)}$  where  $Y = \log(1/x)$  is the total rapidity,  $Y_0$  is the intercept and  $Y_0$  sets the absolute value. Varying  $Q$ ;  $Q R_0 \ll 1$  corresponds to the dilute limit while when  $Q R_0 \gg 1$ , the dipole-proton cross-section saturates to a finite limit. In two-hard-scale problems, one has now to deal with dipole-dipole cross-sections which require an extension [12] of the GBW parametrization. In the case of forward jets, one has to combine these dipole-dipole cross-sections with an appropriate definition of the coupling of this cross-section to the forward jet. This has been proposed in [16]. We shall use this coupling in the analysis of forward jets at HERA.

The QCD cross-section for forward-jet production in a lepton-proton collision reads

$$\frac{d^{(4)}}{dx dQ^2 dx_J dk_T^2} = \frac{s(k_T^2)}{x Q^2} f_{\text{eff}}(x_J; k_T^2) \frac{d_{T,L}}{dk_T^2} (1 - y) + \frac{d_{T,L}}{dk_T^2} \frac{y^2}{2} ; \quad (1)$$

where  $x$  and  $y$  are the usual kinematic variables of deep inelastic scattering,  $Q^2$  is the virtuality of the photon with longitudinal (L) and transverse (T) polarization, and  $x_J$  is the jet longitudinal momentum fraction with respect to the proton.  $d_{T,L} = dk_T^2$  are the photon-parton hard differential cross-sections for the production of a forward (gluon) jet with transverse momentum  $k_T^2$ . Note that we use the usual 1-loop running coupling constant  $s(k_T^2)$  with 4 active flavours, and  $Q_{\text{CD}} = 220 \text{ MeV}$ .

The effective structure function  $f_{\text{eff}}$  has the following expression

$$f_{\text{eff}}(x_J; k_T^2) = g(x_J; k_T^2) + \frac{4}{9} q(x_J; k_T^2) + \bar{q}(x_J; k_T^2) ; \quad (2)$$

where  $g$  (resp.  $q, \bar{q}$ ) are the gluon (resp. quark, antiquark) structure functions in the incident proton.  $k_T^2$  is chosen as the QCD factorization scale.

Properly speaking, the forward-jet cross-section formula (1) is the leading  $\log(1/x)$  expression when one uses the BFKL formulation of  $d_{T,L} = dk_T^2$ : Let us show how one can extend this formalism when saturation corrections are present, e.g. in the framework of the GBW model. The differential hard cross-section reads

$$\frac{d_{T,L}}{dk_T^2} = \frac{\mathcal{G}_{T,L}}{\mathcal{G} Q^2} (Q^2; Q^2) \Big|_{Q = k_T} \quad (3)$$

where  $\tau_{T,L}$  are the cross-sections for the production of a forward jet of transverse momentum larger than  $Q$ ; expressed in the dipole framework by [16]

$$\tau_{T,L}(Q^2; Q^2) = \frac{Z}{2} \int_0^Z d^2r d^2r' \tau_{T,L}(r; Q^2) \tau^J(r; Q^2) \frac{1}{1 + \exp \left( \frac{r_{\text{eff}}^2(r; r')}{4R_0^2(Y)} \right)} ; \quad (4)$$

times the term in brackets in formula (4) is the GBW dipole-dipole cross-section.

$$R_0^2(Y) = \frac{1}{Q_0^2} e^{-(Y - Y_0)} \quad (5)$$

is the saturation radius needed for the forward jet case, namely  $Y = \log \frac{x_T}{x}$ ; the rapidity interval available for the photon-forward jet cross section (see Fig 1), the saturation intercept and  $Y_0$  is a parameter defining the rapidity for which  $R_0(Y_0) = 1 = Q_0 = 1 \text{ GeV}^2$ .  $Y_0$  is the value at which the dipole-dipole cross-section saturates.

The effective radius  $r_{\text{eff}}^2(r; r')$  is defined by

$$r_{\text{eff}}^2(r; r') \lesssim 1 + \ln \frac{r'}{r} = \frac{dd(r; r')}{2 - \frac{2}{s}} ; \quad (6)$$

where  $r^2$  (resp.  $r^2'$ ) is  $m(r; r)$  (resp.  $m(r; r')$ ). As indicated by (6), its expression comes from the elementary dipole-dipole cross-section given by the two-gluon exchange [17]; it appears also in the dilute limit (1st order) of the GBW formula (4).

The functions  $\tau_{T,L}(r; Q^2)$  and  $\tau^J(r; Q^2)$  express the couplings to the virtual photon and to the jet.  $\tau_{T,L}(r; Q^2)$  is the known squared QED wavefunction [18] of a photon in terms of  $q\bar{q}$ . The definition of  $\tau^J(r; Q^2)$  associated with a forward jet with transverse momentum  $k_T > Q$  requires more care [16]. It has been obtained by taking advantage of the equivalence between the partonic and dipole formulations of the jet vertex when it is emitted off an onium (see Fig 2b-2c). In the collinear limit approximation [14, 15, 16], one finds

$$\tau^J(r; Q^2) = \frac{Q}{2r} J_1(Qr) ; \quad (7)$$

Inserting in formula (4) the known Mellin transform  $\sim(\ ) = \int_0^R d^2r (r^2 Q^2)^1 \tau(r; Q^2) :$

$$\sim^J(\ ) = Z^2 \frac{(2)}{(\ )} \quad \sim_{T,L}(\ ) = \frac{2N_c}{q} \frac{X}{e_q^2} \frac{1}{4} \frac{2(1 + \ )^2(1 - \ )^2(2 - \ )}{(2 - 2)(2 + 2)(3 - 2)} \frac{(1 + \ )(2 - \ )}{2(1 - \ )} \quad (8)$$

and after straightforward transformation we can express our results in a double Mellin-transform representation:

$$\frac{d \tau_{T,L}}{dk_T^2} = \frac{Z^2}{8Q^2 k_T^2 R_0^2(Y)} \frac{d}{2i} \sim_{T,L}(\ ) (4Q^2 R_0^2) \frac{d}{2i} \sim^J(1 - \ ) (4k_T^2 R_0^2) \quad \text{if } \sim(\ ; \ ) g : \quad (9)$$

$$0 < \text{Re}(\ ); \text{Re}(\ ); \text{Re}(\ ) < 1 ;$$

where

$$\sim(\ ; \ ) = \int_0^Z \frac{du^2}{du^2} \frac{Z}{du^2 u^2 - 4u^2 - 2} \frac{1}{1 - e^{r_{\text{eff}}^2(u; u)}} = \int_0^Z \frac{2(1 - \ )}{1 + \ } \frac{1}{du u^2 - 1} r_{\text{eff}}^2(1; u)^{1+} \quad : \quad (10)$$

One finally gets, using (6)

$$\sim(\ ; \ ) = \int_0^Z \frac{2(1 - \ )}{1 + \ } f(1; 3 + \ ; 2) + f(1; 3 + \ ; 2 - 2) g ; \quad (11)$$

where the confluent hypergeometric function of Tricomi  ${}_1F_1(1; a; b)$  can be expressed [19] in terms of incomplete Gamma functions.

Expanding the exponential function in the GBW dipole-dipole cross-section in (4), it is possible to single out order by order the contribution of  $r_{\text{eff}}^{2n}$  in formula (9):

$$\sim^{(n)}(\ ; \ ) = 2 \int_0^Z \frac{(-1)^{n-1}}{n!} \frac{1}{2i} ( \ ; \ + n - 1) f(1; 3 + \ ; 2) + f(1; 3 + \ ; 2 - 2) g ; \quad (12)$$

There is an interesting physical interpretation of this expansion.  $\sim^{(1)}$  corresponds to the dilute limit of the GBW formula. Taking also into account  $\sim^{(2)}$  can be interpreted as saturation à la Gribov-Levin-Ryskin [2], i.e.  $r_{\text{eff}}^4 = 8R_0^2(Y)$ .

Note that formulae (9,10) can also be used with the other models for  $r_{\text{eff}}^2$  proposed in the literature [12].

t				Y <sub>0</sub>			N <sub>ZEUS</sub>			N <sub>H1</sub>		<sup>2</sup> (dof)
sat.	0.402	0.036	0.024	-0.82	0.36	0.01	34.3	8.5	7.0	31.7	8.4	8.7 6.8 (11)
weak sat.	0.370	0.32	0.15	8.23	0.48	0.03	1136	272	2	1042	238	78 8.3 (11)

TABLE I: Results of the fits to the H1/ZEUS data for the GBW model. We find two independent solutions showing either significant (1st line) or only weak (line 2) saturation parameters (see text).

### III. FITTING FORWARD JETS

For the fitting procedure, we will use a method allowing for a direct comparison of the data with theoretical predictions. This method has already been applied [20] for a BFKL parametrization of the same  $d/dx$  data at HERA. We shall extend this method to the GBW parametrization (cf. Eq.(9)).

The published data depend on kinematical cuts (see [21, 22]) which are modeled by bin-per-bin correction factors that multiply the theoretical cross-sections. The details of the method is as follows: i) for each  $x$ -bin, one determines [23] the average values of  $x, Q^2, E_J, k_T$  from a reliable Monte-Carlo simulation of the cross-sections, using the Ariadne Monte-Carlo program me [24]. ii) one chooses a set of integration variables over  $d^{(4)}$  in (1) in such a way to match closely the experimental cuts and minimize the variation of the cross-sections over the bin size. The convenient choice of bins for forward jets [20] is

$$\frac{d}{dx} = \frac{Z}{Q^6} \frac{d^{(4)}}{dx dQ^2 dx_J dk_T^2} \quad \frac{1}{Q^2} \quad x_J \quad \frac{k_T^2}{Q^2} ; \quad (13)$$

Note the choice of the variable  $k_T^2 = Q^2$  which is well-suited for the study of two-scale processes. iii) one fixes the correction factors due to the experimental cuts for each  $x$ -bin, by a random simulation of the kinematic constraints with no dynamical input. The list of correction factors for the given set of data and more details on the method are given in [20].

Using these correction factors, we perform a fit of formulae (1-4) to the H1 and ZEUS data using the GBW parametrization (9). The free parameters are the saturation scale parameters and  $Y_0$  (see (5)) and the normalizations which we keep independent for H1 and ZEUS. Note that they are related to the dimensionless factors  $\alpha Q_0^2 e^{Y_0}$ . The obtained values of the parameters and the  $\chi^2$  of the fit are given in Table I and the resulting cross-sections displayed<sup>1</sup> in Fig. 2.

We notice two possible different solutions are obtained which can be characterised by different strength of saturation effects. Both solutions show similar  $\chi^2$  values and resulting cross-sections, and we chose to display only the solution with higher saturation in Fig. 2 (1st line of table I), the other solution would be indistinguishable on that figure. The  $\chi^2$  per dof is quite good (we use only statistical errors to perform the fit). In Fig. 2, we display the result of the fit (full line), together with the results at 1st and 2nd order (resp. dotted and dashed lines) keeping the same values of parameters corresponding to the 1st solution, for which these orders give distinguishable contributions.

Let us now discuss each solution in turn. The 1st solution (see line 1 of Table I) shows a sizeably larger value of than in the GBW model [8] (cf.  $\alpha_{GBW} = 0.288$ ), leading to more significant saturation effects. The value of  $Y_0$  is found to be completely different (cf.  $Y_0^{GBW} = 8.1$ ) but is strongly correlated with the normalization ( $N \propto \alpha Q_0^2 e^{Y_0}$ ). The normalizations for H1 and ZEUS data are found to be compatible. The 2nd solution (see line 2 of Table I) shows values of and  $Y_0$  more compatible with the GBW result, even if remains somewhat larger.

To analyse these features more in detail, we study how the two minima appear order by order in the expansion of the GBW cross-section using formula (12). In Table II, we show the results of the fits when we truncate the expansion up to 1st, second and third order. The 1st order (1st line in Table II), which corresponds to the dilute limit (6), is very close to the weak saturation minimum. At second order, which corresponds to the GLR version of the model, only one minimum appears which is closer to the saturation minimum of Table I.

Comparing the full GBW model (Table I) with its dilute limit (Table II, row 1) shows that the second minimum indeed corresponds to weak saturation effects in forward jets. Indeed, it is known that a mere BFKL description [20]

<sup>1</sup> We follow the same procedure as in Ref. [20], namely one H1 point at  $k_T > 5$  GeV ( $7.3 \cdot 10^{-4}$ ), and four ZEUS points ( $x = 4 \cdot 10^{-4}$ , and the three highest- $x$  points), were not taken into account in the fit. The three highest- $x$  points for ZEUS cannot be described by a small- $x$  approach probably because the  $x$ -value is too high ( $x > 10^{-2}$ ). The other points cannot be described because of large correction factors. Note that similar discrepancies appear also in other types of fitting procedures, e.g. in Ref. [25].

order				$Y_0$	N <sub>ZEUS</sub>			N <sub>H1</sub>			$\chi^2$ (=dof)		
1	0.372	0.066	0.015	—	53.7	10.9	7.6	49.3	11.5	10.4	8.3 (12)		
2 sat	0.452	0.027	0.027	-1.71	0.47	0.01	20.2	5.8	4.9	19.1	5.2	6.0	6.8 (11)
3 (sat.)	0.447	0.025	0.026	-1.56	0.33	0.02	22.2	3.0	5.3	20.9	2.6	6.6	6.8 (12)
3 (weak)	0.374	0.028	0.016	6.85	0.32	0.12	693	110	78	637	94	35	8.2 (12)

TABLE II: Results of the fits to the H1/ZEUS data for the GBW models with different truncations. 1st line: 1st order (no saturation), 2nd line: 2nd order (GLR model), 3rd and 4th line: 3rd order with either significant or weak saturation effects.

of  $\chi^2 = dx$ , similar to the approximation (6), fits well the same data. By contrast, the second and absolute  $\chi^2$  minimum corresponds to fully significant (if not very big) saturation effects.

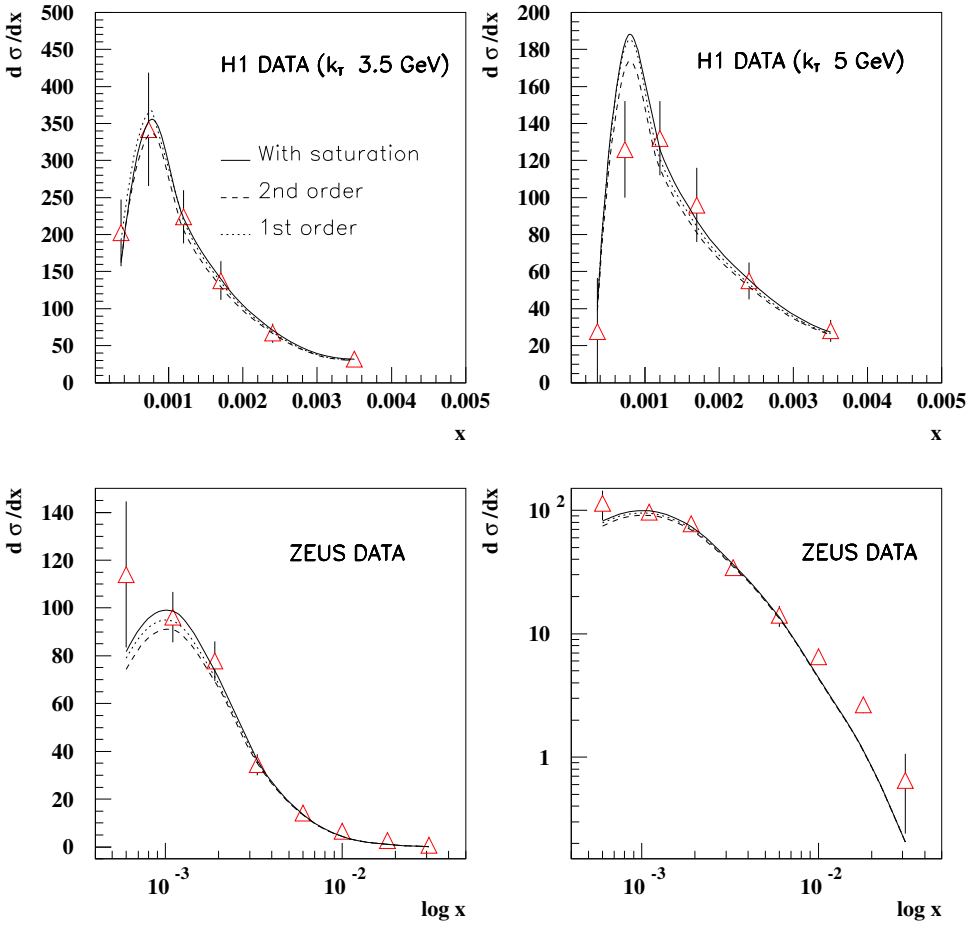


FIG. 2: Results of the fit to the forward jet data with saturation. Upper left: H1 data  $k_T > 3.5$  GeV, upper right: H1 data  $k_T > 5$  GeV, lower left and right: ZEUS data in linear and logarithmic (showing the discrepancy at high- $x$ ) scales. We display the result of the fit in full lines, together with the results at 1st and 2nd order (resp. dotted and dashed lines) keeping the same values of parameters.

Some comments are in order. (i) We always used  $s$  running at one loop in our parametrization, and for completion, we checked the results of the fits while keeping  $s$  constant. We find the same quality of the fits with the effective saturation intercept enhanced by about 30% for the first solution. (ii) We have also studied the other models for

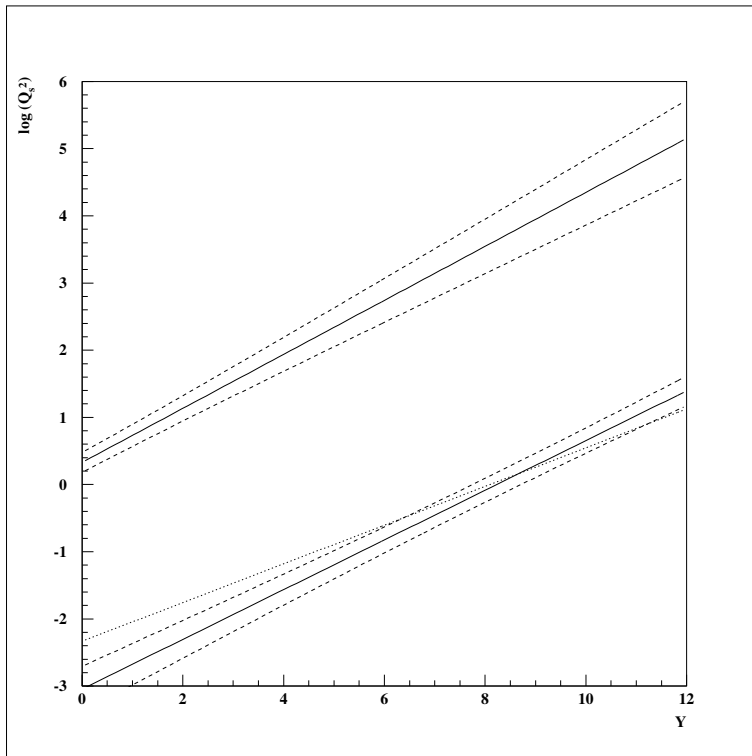


FIG. 3: Saturation scale  $Q_s^2 = 1=R_0^2 = (Y - Y_0)$ . We display the result of the saturation scale for both solutions comparison between the  $F_2$  saturation scale the weak and strong parametrization for forward jets that come out of our fit.

effective radii proposed in Ref. [12] which lead to the same quality of fits with the same values of parameters. (iii) The physical normalization (see Equations (5) and (9)) is  $N \exp(-Y_0)$ . We checked that we obtain a set of consistent values around 50 for this physical normalization for all fits. The discrete values of  $N$  are compensated by the values of  $Y_0$ .

In Fig 3, we plot the different saturation scales as a function of the physical rapidity interval  $Y$ : We also display the saturation scale parametrization obtained by the GBW fit of the proton structure function  $F_2$ . The weak solution is compatible with the one from  $F_2$  in the physical range from five to ten units in rapidity. The rapidity dependence is however somewhat stronger.

At this point it is important to compare the range of  $Q_s^2 = 1=R_0^2 = (Y - Y_0)$  with the experimental transverse momentum cuts. Notice that these cuts (3 and 5 GeV) lie approximately in between the two saturation scale solutions. It is thus clear why the saturation effects are different for both solutions. In particular, the weak saturation minimum can only be due to a sensitivity to fluctuations of the jet dipole distribution (7) around its mean value.

#### IV. PREDICTIONS FOR THE TEVATRON AND THE LHC

The fact that the saturation corrections can be sizeable for two-scale processes suggests that the predictions for related hard cross-sections at hadronic colliders will show striking differences with the weak saturation case. Let us for instance consider the Mueller-Navelet jet production [13] at Tevatron and LHC following the approach of [16]. Indeed, the Mueller-Navelet jet production is directly related to our discussion and, at the level of the two-scale hard cross-section (4), amounts to replacing the photon probe by another forward jet. One writes

$$_{JJ}(k_{T1}; k_{T2}; \Delta Y) = \frac{N_c^2}{16} \int_0^Z d^2r d^2r' \delta^J(r; k_{T1}^2) \delta^J(r'; k_{T2}^2) \frac{1}{1 + \exp \left( \frac{r_{\text{eff}}^2(r; r')}{4R_0^2(\Delta Y)} \right)} ; \quad (14)$$

where  $\Delta Y$  is the rapidity interval between the two jets, and  $k_{T1}$  and  $k_{T2}$  are the lowest transverse momenta of the Mueller-Navelet jets. We thus integrate the differential cross section for  $k_T$  of each jet larger than  $k_{T1}, k_{T2}$ . In order

to appreciate more quantitatively the influence of saturation, it is most convenient to consider the quantities  $R_{i=j}$  defined as

$$R_{i=j} = \frac{(k_{T1}; k_{T2}; \dots; i)}{(k_{T1}; k_{T2}; \dots; j)}, \quad (15)$$

i.e. the cross-section ratios for two different values of the rapidity interval. These ratios display in a clear way the saturation effects. They also correspond to possible experimental observables if one changes the center-of-mass energy since they can be obtained from measurements at fixed values of the jet light-cone momentum and thus are independent of the parton densities in the proton of the incident hadrons. Indeed, such observables have been used for a study of Mueller-Navelet jets for testing BFKL predictions at the Tevatron [20, 26]. However, it is known that hadronisation effects play a role in this kind of measurements and have to be taken into account [27].

In Fig 4, we show the resulting ratios, when  $k_{T1} = k_{T2}$ ; for  $R_{5=2}$  (resp.  $R_{8=2}$ ) which corresponds to accessible rapidity intervals at the Tevatron (resp. the LHC). The curves are for both saturation solutions together with the prediction obtained from the GBW parametrization of  $F_2$ : A clear difference appears in the drop due to saturation which occurs for  $k_T = Q_s = 1 = R_0$ : In particular, the larger value for the saturation case opens the possibility of testing the models at LHC. At even higher scales, both models lead to similar values of  $R$ , larger than the ones extracted [16] from  $F_2$ : This reflects the higher saturation intercept systematically found with forward jets in both cases.

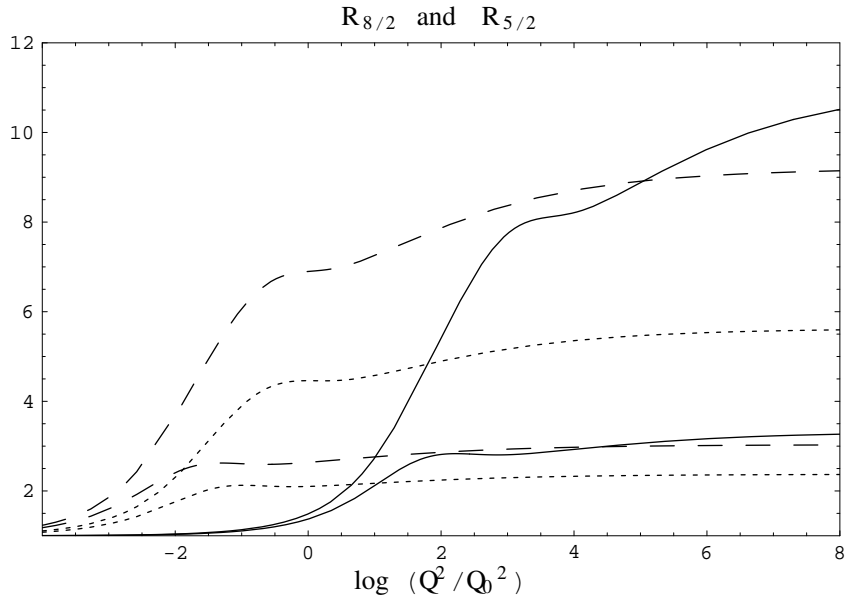


FIG. 4: Cross-section ratios  $R_{i=j}$  between two intervals in rapidity.  $R_{5=2}$  and  $R_{8=2}$  are defined between rapidity intervals 2 and 5 for the Tevatron (lower curves), and 2 and 8 for the LHC respectively (upper curves). The full lines (resp. dashed) are for saturation (resp. weak saturation) solution of Table I. The dotted line comes from the parametrization using the GBW model.

## V. CONCLUSION

Let us briefly summarize the main results of our study. We described the published H1 and ZEUS forward jet data using a saturation model based on the GBW formalism. We find two possible fits to the data with either significant or weak saturation. Both fits lead to different predictions at the Tevatron, or even better at the LHC where the effect is sizeable even for larger jet  $k_T$ . This measurement would imply running the accelerators at different center-of-mass energies. It will allow to test if saturation is stronger for harder processes compared to the proton structure function  $F_2$ . It will be quite interesting to test this model using the recently presented preliminary H1 and ZEUS jet and forward pions data, when they will be available.

---

[1] L. N. Lipatov, Sov. J. Nucl. Phys. 23, (1976) 338; E. A. Kuraev, L. N. Lipatov and V. S. Fadin, Sov. Phys. JETP 45, (1977) 199; I. I. Balitsky and L. N. Lipatov, Sov. J. Nucl. Phys. 28, (1978) 822.

[2] L.V. Grbov, E.M. Levin and M.G. Ryskin, Phys. Rep. 100, (1983) 1.

[3] A.H. Mueller and J. Qiu, Nucl. Phys. B 268, (1986) 427.

[4] L.M. Cierzniak and R. Venugopalan, Phys. Rev. D 49, (1994) 2233; *ibid.*, (1994) 3352; *ibid.*, D 50, (1994) 2225; A.K. Owen, L.M. Cierzniak and H.W. Eigert, Phys. Rev. D 52, (1995) 6231; *ibid.*, (1995) 3809; R. Venugopalan, Acta Phys. Polon. B 30, (1999) 3731; E. Iancu, A. Leonidov and L.M. Cierzniak, Nucl. Phys. A 692, (2001) 583; Phys. Lett. B 510, (2001) 133; E. Iancu and L.M. Cierzniak, Phys. Lett. B 510, (2001) 145; E. Ferreiro, E. Iancu, A. Leonidov and L.M. Cierzniak, Nucl. Phys. A 703, (2002) 489; H.W. Eigert, Nucl. Phys. A 703, (2002) 823.

[5] I. Balitsky, Nucl. Phys. B 463, (1996) 99; Y.V. Kovchegov, Phys. Rev. D 60, (1999) 034008; *ibid.*, D 61, (2000) 074018.

[6] E. Levin and J. Bartels, Nucl. Phys. B 387, (1992) 617; Y.V. Kovchegov, Phys. Rev. D 61, (2000) 074018; E. Levin and K. Tuchin, Nucl. Phys. A 693, (2001) 787; *ibid.*, A 691, (2001) 779.

[7] A.H. Mueller and D.N. Triantafyllopoulos, Nucl. Phys. B 640, (2002) 331.

[8] K. Golec-Biernat and M. Wusthofer, Phys. Rev. D 59 (1998) 014017, Phys. Rev. D 60 (1999) 114023.

[9] G. Altarelli and G. Parisi, Nucl. Phys. B 126 18C (1977) 298. V.N. Gribov and L.N. Lipatov, Sov. Journ. Nucl. Phys. (1972) 438 and 675. Yu. L.D. Okshitzer, Sov. Phys. JETP 46 (1977) 641. For a review: Yu. L.D. Okshitzer, V.A. Khoze, A.H. Mueller and S.I. Troyan Basics of perturbative QCD (Editions Frontières, J.Tran Thanh Van Ed. 1991).

[10] A.H. Mueller, Nucl. Phys. Proc. Suppl. B 18C (1990) 125; J. Phys. G 17 (1991) 1443.

[11] M. Kozlov and E. Levin, Eur. Phys. J. C 28 (2003) 483.

[12] N. Tmeanu, J. Kwiecinski and L. M. Cierzniak, Eur. Phys. J. C 23 (2002) 513, Acta Phys. Polon. B 33 (2002) 1559 and 3045.

[13] A.H. Mueller and H. Navelet, Nucl. Phys. B 282 (1987) 727.

[14] R. Peschanski, Mod. Phys. Lett. A 15 (2000) 1891.

[15] S. M. Unier, Phys. Rev. D 63 (2001) 034015.

[16] C. M. Arquett and R. Peschanski, Phys. Lett. B 587 (2004) 201.

[17] A.H. Mueller, Nucl. Phys. B 415 (1994) 373; A.H. Mueller and B. Patel, Nucl. Phys. B 425 (1994) 471; A.H. Mueller, Nucl. Phys. B 437 (1995) 107.

[18] J.D. Bjorken, J. Kotog and Soper, Phys. Rev. D 3 (1971) 1382.

[19] A.P. Rudnikov, Y.B. Rychkov, and O.M. Marichev, Integrals and Series (Gordon and Breach Science Publishers, 1986).

[20] J. G. Contreras, R. Peschanski and C. Royon, Phys. Rev. D 62 (2000) 034006; R. Peschanski and C. Royon, Pomeron intercepts at colliders, Workshop on physics at LHC, hep-ph/0002057.

[21] H1 Collaboration, C. Adloff et al, Nucl. Phys. B 538 (1999) 3.

[22] ZEUS Collaboration, J. Breitweg et al, Eur. Phys. J. C 6 (1999) 239.

[23] J.G. Contreras, Phys. Lett. B 446 (1999) 158.

[24] L. Lonnblad, Comp. Phys. Comm. 71 (1992) 15.

[25] J. Kwiecinski, A.D. Martin and J.J. Outhwaite, Eur. Phys. J. C 9 (1999) 611.

[26] D0 Collaboration: B. Abbott, et al, Phys. Rev. Lett. 84 (2000) 5722.

[27] J.R. Andersen et al, JHEP 0102 (2001) 007, and references therein.